JSMT

http://publisher.uthm.edu.my/ojs/index.php/jsmt

e-ISSN : 2821-2835

Journal of Sustainable and Manufacturing in Transportation

A Study of Weld Seams on Low Carbon Steel ABS Grade a Marine Plates Using SMAW Process

Lester Chin Zen Kai[1], Sung Aun Naa[2*], Edwin Jong Nyon Tchan[3]

[1]Department of Mechanical Engineering, Faculty of Engineering and Science,
Curtin University, Malaysia, 89009 Miri, Sarawak, MALAYSIA

[2]School of Engineering,
Vitrox College, 746, Persiaran Cassia Selatan 3, 14110 Batu Kawan, Pulau Pinang, MALAYSIA

[3]Department of Petroleum Engineering, Faculty of Engineering and Science,
Curtin University Malaysia, 89009 Miri, Sarawak, MALAYSIA

*Corresponding Author

DOI: https://doi.org/10.30880/jsmt.2023.03.01.002
Received 6 May 2023; Accepted 5 July 2023; Available online 31 July 2023

Abstract: Understanding the impact of welding parameters and welder skill on weld quality is crucial. However, it is the lack of comprehensive studies that consider the welding parameters and welder-introduced defects when analyzing the mechanical and metallurgical behaviors of low carbon steel welds using the SMAW process. The research aims to study and assess the impact of weld seams of low carbon steel ABS Grade A marine plate of 12.7mm thick using manual SMAW process as per AWS D1.1 structural welding code requirements and fulfilments of ASME Section IX pressurized equipment welding code requirements too. Different voltages, currents, and travel speeds were used to weld the test specimen plates. After the manual SMAW process, a series of testing techniques, including non-destructive tests, such as VT and RT, and destructive tests, such as tensile tests, bend tests, impact tests, microhardness tests, and metallographic examination has been conducted to assess/evaluate on the welded seam profiles and analyses/determines whether the accepted welded seam profiles have fulfilled the relevant welding code requirements. From the series of assessments and analyses, it is confirmed that the welded test specimen 1 having the welding parameters (i.e., voltage 23 V, current 70 A, and travel speeds 56.52 – 312.50 mm/min, having a range of heat inputs from 0.31kJ/mm to 1.71kJ/mm) is accepted as the quality good weld seam.

Keywords: Shielded Metal Arc Welding, SMAW, low carbon steel, welding parameters, heat input, non-destructive test, destructive test

1. Introduction

Welding is a process used to permanently join two or more pieces of metal. Among the different welding processes, Shielded Metal Arc Welding (SMAW) is widely used in industrial application [1]. SMAW welding provides cost-effective maintenance and equipment, easy electrode changeability, welding in confined spaces, no need for shielding gas, faster deposition rates compared to GTAW, and good portability [2]. The ISO 9606-1 qualification for fusion welding of steels encompasses factors such as the welding process, type of part (plate or pipe), welding joint (butt or fillet), filler material group and type, dimensions of the part (tube thickness and outside diameter), welding position, welding details (e.g., gas by root side, one-side welding, single pass), and base material group [3]. The heat input during welding is also a critical factor that affects weld quality. Welding current, voltage, and electrode travel speed all play a role in controlling heat input. The level of welding current used affects the mechanical properties of the melting zone [4], while the type of

*Corresponding author: aun-naa.sung@vitrox.com

welding power sources used are correlated with the appearance of the weld beads [5]. However, no previous studies have reported on the selection of those welding parameters using SMAW process to join low carbon steel ABS grade A marine plate.

Several researchers have conducted studies on the mechanical behavior and microstructure of low steel carbon pipes after undergoing the SMAW process. De Sousa Lins [6] studied the mechanical properties of 0.08 wt% C after undergoing the SMAW process. Similary, Boumerzoug et. al [7] conducted a study on the effect of SMAW on the microstructure of low carbon steel pipe with 0.19 wt% C by comparing the microstructure of the low carbon steel pipe before and after SMAW process. They investigated the hardness of low carbon steel after SMAW but did not provide information on welding parameters, such as welding current, welding voltage, and travel speed. Talabi et.al [8] investigated the effect of welding parameters, including welding voltage, welding current, welding speed, and electrode diameter, on the mechanical behavior of the low carbon steel with 0.08 wt% C using SMAW process. The mechanical behaviors investigated including ultimate tensile strength, yield strength, impact strength, and hardness behaviors. Sixteen graphs are plotted based on the four welding parameters and the four mechanical behaviors. However, the information about the four welding parameters for each test specimen has not been stated. For instance, Asibeluo [9] studied the effect of welding current on the hardness, impact toughness, and microstructure of A36 carbon steel 0.26 wt% C using SMAW process. There is no information on welding voltage and travel speed in the study. From the abovementioned studies, the information of welding parameters has not been listed and thus the welds are not producible.

Previous research has examined the mechanical behaviors and microstructures of low carbon steel using SMAW process with both high and low heat inputs. Gharibshahiyan et. al [10] investigated the grain size and hardness of low carbon steel 0.06 wt% C using SMAW process with high heat inputs of 54 kJ/mm and 81 kJ/mm. Similarly, Kolhe et al. [11] studied the hardness, impact toughness, and microhardness of a multipass welded joint of low carbon steel 0.25 wt% C using submerged arc welding (SAW) process with low heat inputs of 1.47 J/mm and 3.0 J/mm. However, it should be noted that such a range of heat inputs is not practical when welding carbon steel materials.

Muda et al. [12] conducted an experiment to investigate the effect of heat input on the mechanical properties and microstructure of ABS Grade A steel with 0.17 wt% C. The study examined three different heat inputs ranging from 0.99 kJ/mm to 2.25 kJ/mm and evaluated the impact toughness and hardness of the welded cap. However, the study did not include impact testing at sub-zero temperatures, which is crucial for determining the material's behavior below the ductile to brittle transition temperature. Additionally, the study neglected to investigate the hardness of the ABS Grade A steel at the root of the weld, focusing solely on the cap.

In addition to welding parameters, the skill level of the welder is a crucial factor that impacts weld quality. SMAW requires highly trained welders [13]. Various defects such as porosity, lack of fusion, incomplete fusion, entrapped slag, and poor bead shape can be introduced by the welder. In previous studies, the mechanical properties and microstructures of low carbon steel welds were analyzed without considering the possible defects introduced by the welders. These defects can significantly affect the mechanical behaviors of the weld. Therefore, there is a need to conduct studies on the mechanical behaviors and microstructures of welds by eliminating the defects introduced by the welder.

This study has two main objectives. The first objective is to identify and establish optimal SMAW parameters that can consistently produce high-quality welds for multiple passes. The second objective is to analyze and evaluate the metallurgical and mechanical behaviors of the weld. The material used in this study is a 12.7 mm thick low carbon steel plate with 0.16 wt% C, which is manufactured from ABS Marine Steel Plate Grade A. To ensure the quality of the welds, the possible defects introduced by the welder are examined using non-destructive tests (NDT), including visual inspection (VT) and radiographic testing (RT). Additionally, the test specimen is subjected to macro-etching and metallographic examination, as well as destructive testing (DT), including tensile testing, bend testing, Charpy V-notch impact testing, and microhardness testing.

2. Methodology

The process flow chart of the research methodology is presented in Figure 1. In Step 1, the base materials were prepared by oxy-cutting, beveling to the required bevel angle, grinding, and cleaning. Eight low carbon steel ABS Grade A marine plate were sectioned, each with dimensions of 200 mm × 140 mm × 12.7 mm, using an oxyacetylene cutter. The chemical composition and mechanical properties of the ABS Grade A plate were obtained from the mill certificate, as shown in Table 1. Preheating was not carried out in this experiment since low carbon steels with thickness less than 1 inch do not require preheat. A 30º bevel angle of a single V groove with a root opening of ±3 mm and root face thickness of ±2.0 mm was machined at the edge of the steel plates. After beveling, grinding, and cleaning, two tack welds, each 20 – 25 mm long, were made to align the two steel plates in the proper location before welding commenced.

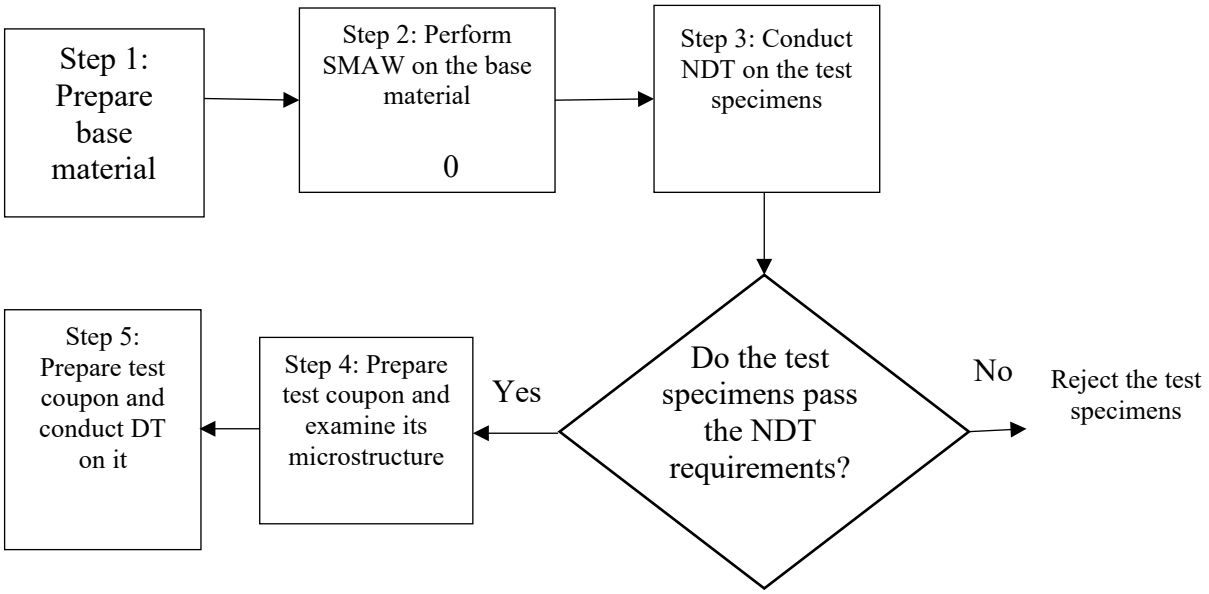

Fig. 1 - Flow chart of methodology

In Step 2 of the methodology, SMAW was performed on the eight steel plates to generate four test specimens The four test specimens were welded with multiple passes using different combinations of welding parameters, such as current, voltage, electrode travel speed, and type of electrode, as outlined in Table 2. The objective was to identify the optimal combination of parameters for achieving good quality welds. The welding passes for the single V-Groove configuration consisted of four passes: root, hot, fill, and cap passes, in a predetermined sequence specified in the p-WPS. The travel speed was dependent on the skill of the welder, and was calculated for each pass by measuring the electrode travel distance and travel time. The skilled welder used a weaving or stringing motion, with the electrode moved uniformly from side to side at an inclination of 5° to 15° in the direction of the weld. The test specimens were welded according to the AWS D1.1 Structural Welding Code – Steel [14].

Table 1 - Chemical compositions and mechanical properties of the test specimens in mill certificate

Chemical Elements					Yield Strength, MPa	Tensile Strength, MPa	Elongation, %
C	Mn	Si	P	S			
0.16	0.96	0.20	0.012	0.004	342	491	32

Table 2 - The welding parameters of 4 specimens

Independent Variables					Dependent Variables			
Test specimen	Weld Layer	Electrode & current polarity	Voltage (V)	Current (A)	Travel time (s)	Travel distance (mm)	Travel speed (mm/min)	Heat input (kJ/mm)
1	Root	E7016 & DCEN	23	65	80	80	66.66	1.35
					70	70	59.49	1.51
	Hot				65	100	95.24	0.94
					29	30	103.45	0.87
					26	20	76.92	1.17
	Fill 1	E7018 & DCEP			82	150	122.95	0.73
	Fill 2a				85	150	120	0.75
	Fill 2b				81	150	123.97	0.72
	Fill 3a				79	140	117.64	0.76
					12	10	83.33	1.08
	Fill 3b				77	150	128.21	0.70
	Cap a				67	110	102.80	0.87
					19	40	210.53	0.43
	Cap b				58	110	189.66	0.47
					23	40	173.91	0.52

2	Root	E7016 & DCEN	23	65	80	85	70.83	1.36
					75	65	56.52	1.71
	Hot				90	120	92.30	1.05
					25	30	120.00	0.81
	Fill 1	E7018 & DCEP			89	150	116.28	0.83
	Fill 2				92	150	113.64	0.85
	Fill 3a				70	105	95.45	1.01
					7	45	642.00	0.15
	Fill 3b				68	90	83.33	1.16
					9	60	666.67	0.14
	Fill 4a				77	150	128.21	0.75
	Fill 4b				78	140	118.64	0.81
					5	10	200.00	0.48
	Cap A				76	135	116.38	0.83
					17	15	88.24	1.09
	Cap B				59	80	135.59	0.71
					42	70	166.67	0.58
	Cap C				48	150	312.50	0.31
3	Root	E7016 & DCEN	20	80	67	75	70.09	1.37
					62	45	44.12	2.18
					27	30	111.11	0.86
	Hot				71	100	90.09	1.07
					41	50	121.95	0.79
	Fill 1	E7018 & DCEP			68	90	83.33	1.15
					50	60	120	0.80
	Fill 2a				66	120	113.20	0.85
					9	30	333.33	0.29
	Fill 2b				49	90	183.67	0.52
					36	60	166.67	0.58
	Cap A				70	140	127.27	0.75
					12	10	83.33	1.15
	Cap B				59	110	186.44	0.51
					19	40	210.53	0.46
4	Root	E7016 & DCEN	19	90	59	75	127.11	0.81
					56	60	107.14	0.96
					10	15	150	0.68
	Hot				69	90	82.57	1.24
					36	60	166.67	0.62
	Fill 1	E7018 & DCEP			61	100	99.01	1.04
					32	50	156.25	0.66
	Fill 2a				65	110	104.76	0.98
					28	40	142.86	0.72
	Fill 2b				66	90	84.91	1.21
					28	60	214.29	0.48
	Cap A				64	140	134.62	0.76
					12	10	83.33	1.23
	Cap B				64	135	129.81	0.79
					16	15	93.75	1.09

The power source used had a constant voltage (CV) with direct current electrode negative (DCEN) and/or with direct current electrode positive (DCEP). Direct current was selected over alternating current (AC) as AC produces more spatters and unstable welding current [13]. DCEN provided better and deeper penetration, while DCEP provided a wider weld with shallower penetration. The E7016 and E7018 low hydrogen iron powder electrodes were selected for the SMAW process to minimize the risk of gas (i.e., hydrogen) entrapment. The E7018 electrode with DCEP was selected for root and hot passes, while the E7018 electrode with DCEN was used for the fill and capping of the weld seam. The electrode diameter was chosen as 2.6 mm to produce a lower welding current and minimize dilution. In order to achieve a higher deposition rate, additional iron powder was coated onto the rimming steel wire, which produced a larger weld

puddle to cushion the arc and this increased the likelihood of slag inclusion. Thus, every layer of weld metal was cleaned and ground thoroughly to remove all possible deposited slags before the deposition of the next layer of weld metal.

In Step 3 of the methodology, NDT techniques, such as VT and RT, were conducted on the welded test specimens. VT was performed during welding to identify any potential surface discontinuities and defects, while RT was conducted to assess any possible sub-surface anomalies. These tests are commonly used in industry and were carried out in compliance with DNV Standard for Certification 2.7-1 [15] and the requirements of ASME Section V [16].

During VT, the certified welding inspector (CWI) with trained good eyesight carried out the inspection and moved around for effective VT as per the AWS D1.1 standard [14]. The luminous emittance during VT was maintained at 1000 Lux (100 fc) per ASME Section V Article 9 [16]. The welded test specimens were placed at a distance of 600 mm from the inspector. VT was performed on the weld root, each weld pass, and the entire weld seam to assess the regularity/smoothness of the weld during and after welding. Defects on the weld root pass, hot pass, and subsequent passes were checked during welding, while surface defects on the weld seam were re-examined after welding.

After VT screening, RT was performed to identify any subsurface defects in the weldment. The test specimens were placed between penetrating radiation and X-ray films, along with a chosen Image Quality Indicator (IQI) sensitivity. The detected radiographic image captured the intensity of radiation that penetrated the test specimen. RT was carried out in compliance with ASME Section V Article 2 for radiographic examination and Article 22 for radiographic testing standards [16].

In Step 4, the test specimen that met the acceptance criteria of NDT requirements underwent metallographic analysis. A selected test coupon was machined from the welded flat surface to assess various mandatory DT requirements. The flat surface was prepared by cutting, mounting, grinding, cleaning, and polishing to a 1 μm mirror-like finish to ensure no visible detectable defects. The test coupon was then etched with an appropriate etchant to reveal the microstructures across the weldment and further assess any possible subsurface anomalies. Macrostructure examination was conducted using optical microscopes with a 10 × magnification across the weldment, while microstructure examination was performed with a magnification of 100 × and 500 ×. The macrostructure examination was carried out in accordance with ASTM E340 [17], and one image was captured for macrostructure examination. Additionally, seven images of the test coupon were taken, including regions encompassing weld metal, HAZ, and base metal, as depicted in Figure 2.

In Step 5, the test coupons were subjected to mandatory DT, including traverse tensile tests, bending tests, Charpy V-notch impact tests, and microhardness tests, to evaluate the achievable mechanical properties of the weld metal. The test coupons for DT were carefully prepared from the defect-free welded test specimen after undergoing the mandatory NDT assessments. The test couples for DT consist of weld metal, HAZ, and base metal.

A transverse tensile test was conducted using a Gotech computerized universal testing machine, model GT-7001-LC-50. The force and elongation of the test coupon were measured to obtain the tensile strength and compared with the tensile strength given by the original mill certificates listed in Table 1. Two transverse test coupons were machined to a reduced section, with dimensions of 11.55 mm thickness, 16.00 mm width, and 184.80 mm^2 effective area. A stress-strain curve was obtained from the test. The tensile test was carried out in accordance with the American Standard for Testing Materials, ASTM A370, at a test temperature of 25 ºC [18].

The bend test was conducted to determine the ductility of the welded joints, in compliance with the American Standard for Testing Materials, ASTM E190 [19]. Two test coupons with a width of 10 mm and thickness of 12.7 mm were prepared from the side surface of the test specimen. The test coupons were placed on the bending jig on top of the rounded shoulders, and a side bend test with a bend angle of 180° was carried out using the Fukunaga Hydraulic Machine, model FEP-IDS, at a test temperature of 25°C, according to ASME IX welding codes requirements [20].

The Charpy V-notch impact test was conducted in accordance with the ASTM E23 standard [21]. The Avery Denison Model IMP 300CA Charpy impact tester was used for the test. Four sets of test coupons, with dimensions of 55 mm × 10 mm × 10 mm, were prepared for the test. The ductile brittle transition temperature for ABS Grade A steel plate is -42 ºC [22]. Therefore, the impact test was performed at sub-zero temperatures of -29 ºC and -50 ºC. Liquid nitrogen was used to achieve the sub-zero temperatures, and the test coupons were soaked in it for 20 minutes to stabilize them at the required testing temperature. The energy absorbed in Joules (J) by the test coupon was calculated from the pendulum height, and the notch toughness at the weld metal of the test coupon was determined based on the energy absorbed.

In accordance with ASTM E384-16 requirements [23], a microhardness test was performed to determine fine-scale changes in the microhardness values of the weldment. The Akashi Vickers Hardness Tester, Model AVK-C100, was used to measure the microhardness values of the weldment across the cap and root sections at seventeen points for each section, as shown in Figure 2. The load was applied smoothly without impact and held for 10 to 15 seconds, with an indenter of an included angle of 136°. After removing the load, the two impression diagonals of a square-shaped pyramid diamond indenter were measured using a filar micrometer to the nearest 0.1 μm. The Vickers hardness (HV) was calculated using the following equation:

$$\mathrm{HV} = \frac{1854.4\mathrm{L}}{\mathrm{d}^2} \quad (1)$$

where L= load (grams-force) and d = average diagonal length (μm)

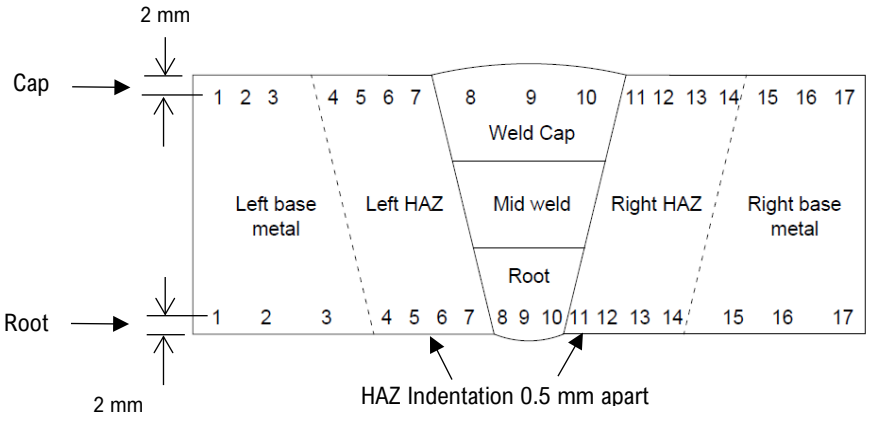

Fig. 2 - The different regions of weld

3. Results and Discussion

3.1 Heat Input Produced Based On The Welding Parameters

Table 2 presents the welding parameters used to produce multiphase for four test specimens. The electrode travel speed was determined by measuring the welding travel distance during each pass within the recorded specific time. The Heat Input, defined as the energy transferred per unit length of a weld, was calculated by dividing the power by the velocity of the heat source. The welding voltage E (V), welding current I (A), and travel speed v (mm/min) were used to calculate heat input H (Joules/min) for each welding pass based on Eqn. (2). Heat input affects the cooling rate which will also influence the mechanical properties and microstructures of the weldment.

$$H = \frac{60 \times E \times I}{1000 \times v} \qquad (2)$$

3.2 Non-Destructive Test Results

3.2.1 Visual Inspection Test Result

Visual inspection of the weld seam is an essential step to detect surface irregularities and weld discontinuities. Figure 3(a) shows a weld seam produced at 65 A, which is irregular and not aligned. There are visible undercut and porosity, and a small amount of spatter is present on the base metal around the weld seam. On the other hand, Figures 3(b) and (c) show weld seams produced at 70 A and 80 A, respectively, with consistent weld bead width and no visible defects. The weld reinforcement of both specimens is less than 3 mm at an angle less than 30°, which is acceptable according to the AWS D1.1 standard. Figure 3(d) shows a weld seam with all passes evenly distributed, and the surface of the weld seam is smooth with a constant/evenly distributed weld profile. However, some minor porosity, which is the cavity type discontinuities due to gas bubble entrapment during solidification of the weld, is found. This type of defect can be caused by various factors such as insufficiently dry electrodes in high humidity or excessive moisture present in the flux. Nonetheless, the test specimen is still considered acceptable after the NDT-RT assessment.

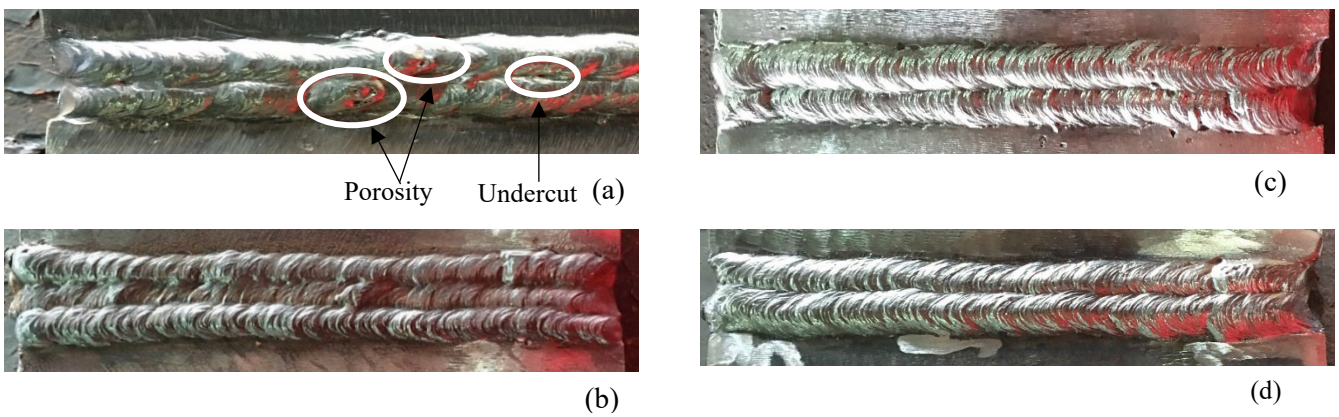

Fig. 3 - Pattern of Weld Seam after welding for specimens welded with (a) 65A; (b) 70 A; (c) 80 A and; (d) 90 A

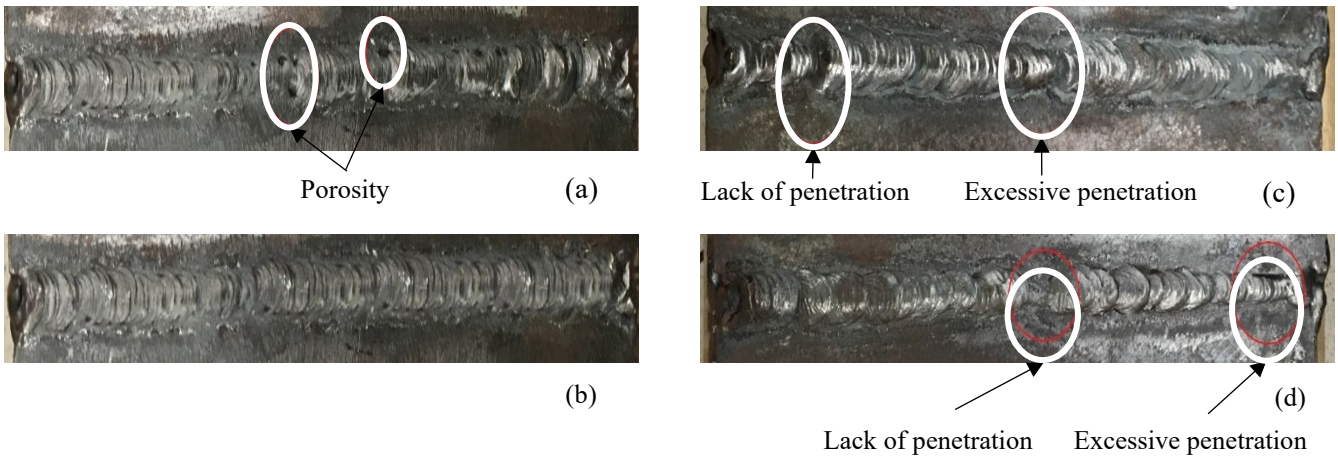

Fig. 4 - Pattern of Weld Root during welding for specimens welded with (a) 65A; (b) 70 A; (c) 80 A and; (d) 90 A

Figures 4(a)-(d) depict the weld root observed during the welding process. The root weld produced with 65 A exhibited visual defects, such as weld concavity and porosity, as shown in Figure 4(a). Despite the concavity being less than 2 mm, the specimen failed to meet the acceptance criteria for visual inspection, as per the specifications of AWS D1.1 and ASME Section IX, due to the porosity at the root of the weld. On the other hand, the weld seam of the root welded with 70 A, as illustrated in Figure 4(b), had a smooth contour, was defect-free, and had a weld concavity of less than 2 mm. Consequently, this specimen met the acceptance criteria for visual inspection. The weld seam of the root welded with 80A, shown in Figure 4(c), displayed excessive and lack of root penetration but was still accepted. In contrast, as observed in Figure 4(d), the root welded with 90A had visual defects, including excessive and lack of root penetration and porosity, and did not meet the NDT test standard requirements after the NDT-RT evaluation.

3.2.2 Radiographic Test Result

X-ray films of the specimens obtained from the radiographic test are presented in Figures 5(a)-(d). Darker shadows on the films indicate the presence of defects and hidden flaws, as more radiation passes through. Based on the X-ray films, the specimens produced with 65 A and 90 A (Figure 5(a) and (d), respectively) were rejected due to the presence of a slag line and both slag line and cluster porosity, respectively, at the sub-surface of the weld seam. On the other hand, the specimens produced with 70 A and 80 A (Figures 5(b) and (c)) were accepted. The specimen produced with 70 A exhibited no defects, while the specimen produced with 80 A was accepted despite having cluster porosity in a 1 cm.

3.3 Metallographic Examination

Based on the NDT results, only the specimen welded with 70 A was acceptable. Therefore, this specimen was further evaluated by microstructure examination and DT. Figure 6 shows an image of the test coupon observed under 10× magnification, with no defects found and the coupon was accepted. The microstructure of the weldment was examined using an optical microscope with a magnification of 100×, and the image is shown at the center of Figure 7. Based on the regions listed in the image, microstructures of various regions under a magnification of 500× were obtained and shown in Figure 7 as well.

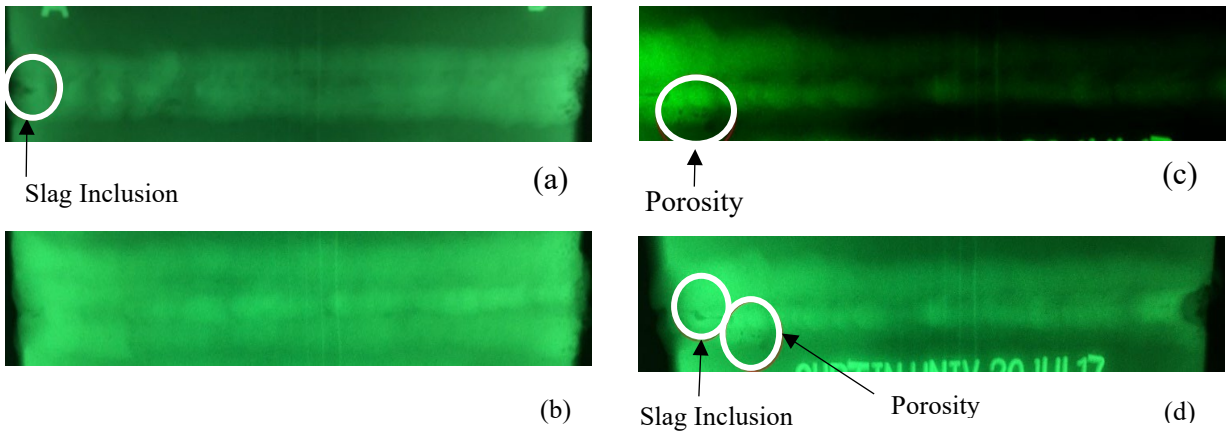

Fig. 5 - X-Ray Films for specimens welded with (a) 65A; (b) 70 A; (c) 80 A and; (d) 90 A

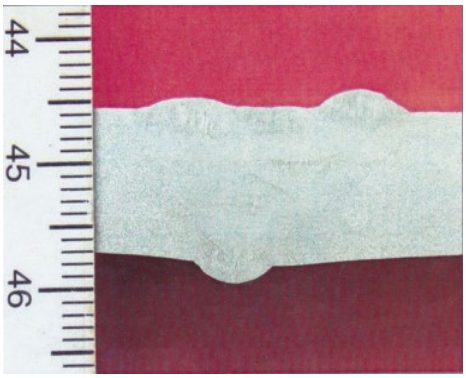

Fig. 6 - The macro-photograph of the test coupon welded with 70 A with magnification of 10 ×

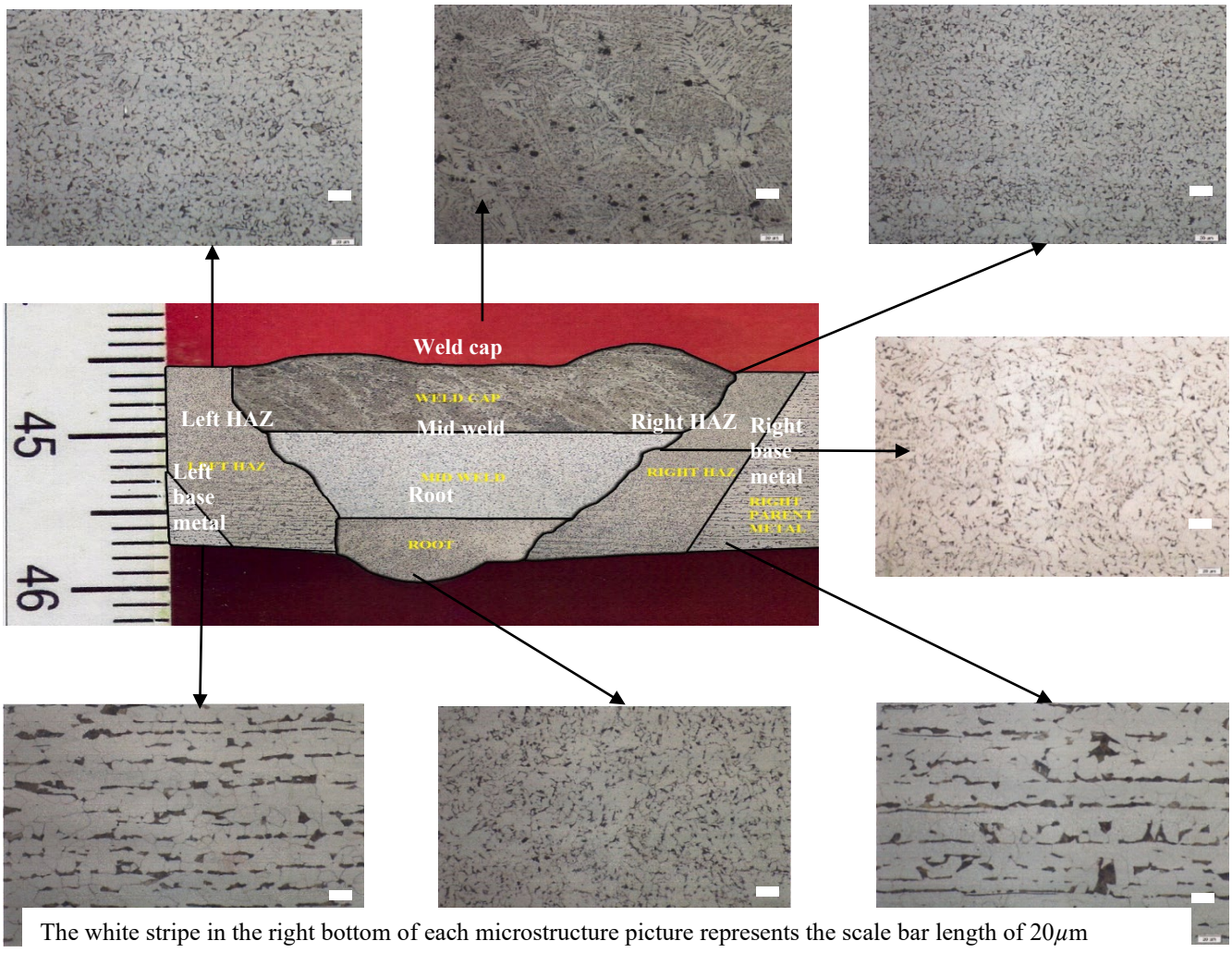

The white stripe in the right bottom of each microstructure picture represents the scale bar length of 20μm

Fig. 7 - Results of the microstructure examination for various regions of the test coupon welded with 70 A

The microstructure analysis revealed that there was a complete change in microstructures across the weldment, from the base material's microstructures with the mixture of ferritic phases and pearlite phases. The weld metal had completely melted and solidified forming needle-like (Widmannstetter) structures that interlocked with each other with no visible defects, even under high magnification views. However, the weld cap passes had coarser structures compared to the root passes. This may be due to the repeated heating and cooling cycles of the root passes generating from the subsequent passes, including hot passes and inter-fill passes, while the cap passes only had one heating and cooling cycle.

Immediately following the weld metal, there were the fusion lines and the heat-affected zones (HAZ) on both sides of the weld metal. It was further observed that the weld metal, fusion lines, and adjacent HAZ were fully fused together

with no identified defect. However, the microstructures in the HAZ were relatively different from those near the fusion lines and those in the base metal.

The test coupon showed varying grain sizes and structures across different regions due to differences in received heat inputs. The weld metal had the finest grain size, followed by the HAZ and base metal due to its higher cooling rate and lower heat input. This finding is consistent with the results of previous studies by Boumerzoug et al. [7] and Choubey and Jatti [24]. The microstructure of the weld cap, shown in Figure 8, contains ferrite, pearlite, and acicular ferrite. Ferrite is the primary component of carbon steel at room temperature, while austenite transforms into ferrite during cooling. Carbon combines with ferrite to form pearlite, which appears darker due to its lamellar structure. The formation of martensite, cementite, pearlite, and retained austenite, as well as differences in grain size, can affect the mechanical properties of the weldment, such as hardness and toughness. Lower heat input in the weld metal can result in increased hardness and impact toughness.

3.4 Destructive Test Result

3.4.1 Tensile Test Result

The test coupon, as seen in Figure 9(a) after the tensile test, fractured at the base metal. Based on Figure 9(b) and the stress-strain curve in Figure 10, the test coupon undergoes moderate ductile fracture with plastic deformation after exceeding the yield point. This fracture location is acceptable as it confirms the higher tensile strength of the weld metal compared to the base metal.

To meet the requirements of ASME Section IX [20], the weld metal's tensile strength should be higher than the base metal's minimum tensile strength. According to Table 1, the base metal's minimum tensile strength is 491 MPa, while the weld metal's tensile strength, calculated from the stress-strain curve in Figure 10, is 522 MPa. As the test coupon's ultimate tensile strength is greater than the base metal's minimum specified value, it meets the ASME Section IX requirements [20]. The yield strength, which exceeds the minimum requirement for carbon steel yield strength in ASME Section IX [20], is 289.08 MPa, as shown in Figure 10.

3.4.2 Bend Test Result

The weldment was subjected to a bend test in accordance with ASME Section IX welding codes, which require the maximum allowable discontinuity to be less than 3 mm [20]. As shown in Figure 11, the test coupon did not break during the test, and a smooth surface with a 2.8 mm opening was observed. This opening falls within the acceptable range. Despite passing visual inspections and X-ray film inspections with no defects found, the weldment still experienced cracking during the bend test.

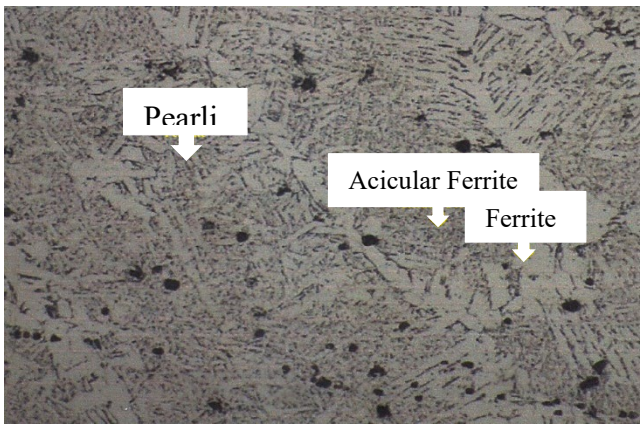

Fig. 8 - Presence of pearlite, acicular ferrite and ferrite

(a) (b)

Fig. 9 - Test coupon (a) after tensile test; (b) cross section view of test coupon after tensile test

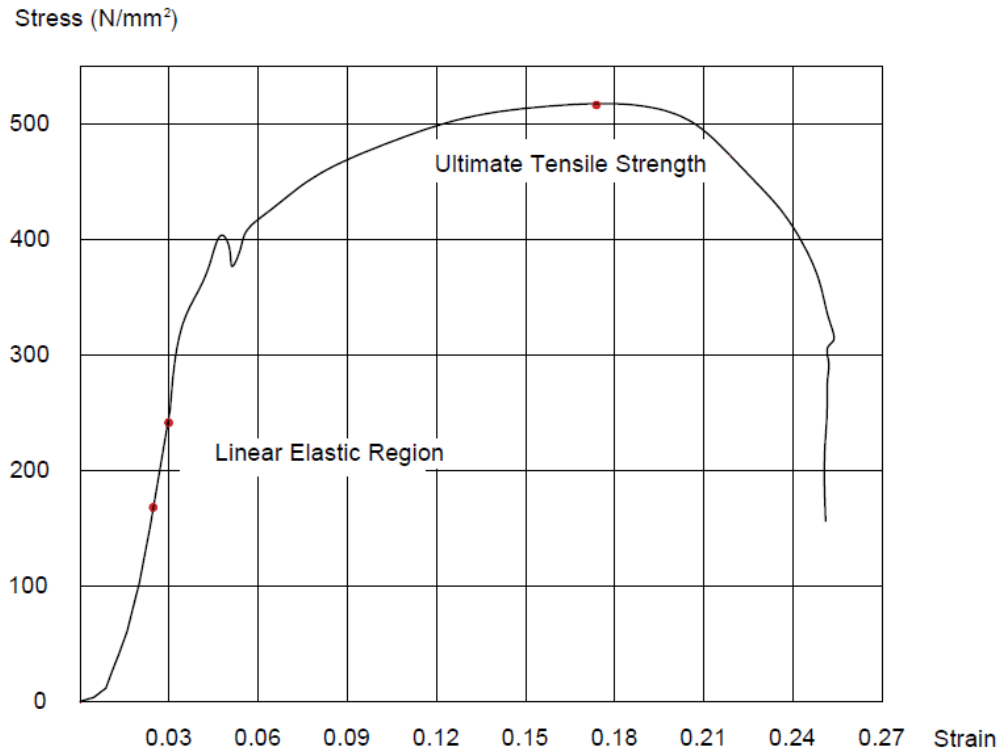

Fig. 10 - Stress-strain curve

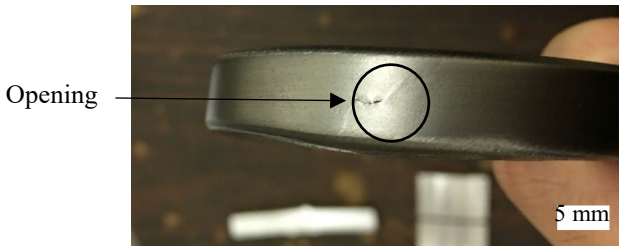

Fig. 1 - The test coupon after bend test

The accumulation of bend strain was found in the heat-affected zone, indicating that the weld metal is stronger than the base metal. This was evidenced by the fact that the weldment did not break, while the base metal experienced strain, resulting in a smooth surface in the middle of the specimen.

3.4.3 Charpy V-Notch Impact Test Result

Table 3 displays the average impact energy obtained from the Charpy V-notch impact test. The average impact energy is calculated from the average value of two test coupons for each test temperature. These values meet the minimum requirements specified in ASME Section IX [18]. Figure 12(a) and Figure 12(b) depict the test coupons before and after the Charpy impact test, respectively. As observed in Figure 12(b), all the test coupons were completely broken into two halves after the test. The dull breaking surfaces indicate the occurrence of ductile fracture, and fibrous pullouts are observed at the breaking surface, showing deformation before fracture. These observations support the results of the tensile test. The impact energy decreases as the test temperature decreases, as shown in Table 3. This is due to the presence of ferrite in the body-centered cubic (BCC) metals, indicating brittleness during low temperatures.

3.4.4 Microhardness Test Result

Figure 13 displays the Vicker hardness (Hv) values obtained at 17 points in the welding cap and root, which are grouped into five regions (left base metal, left HAZ, weld metal, right HAZ, and right base metal) as indicated in Figure 2. The hardness of the weld metal is the highest among all the five regions for both cap and root, as shown in the figure. As the distance of each region from the weld metal increases, the hardness decreases. This distribution of hardness indicates acceptable weld quality since the weld metal is harder than the other regions. The microstructure examination

also supports this finding, and the highest hardness of the weld metal is attributed to its finest grain size. These results align with the tensile test results, where the test coupon broke at the base metal instead of other regions of the weld.

(a) (b)

Fig. 12 - Test coupon (a) before and; (b) after Charpy Impact Test

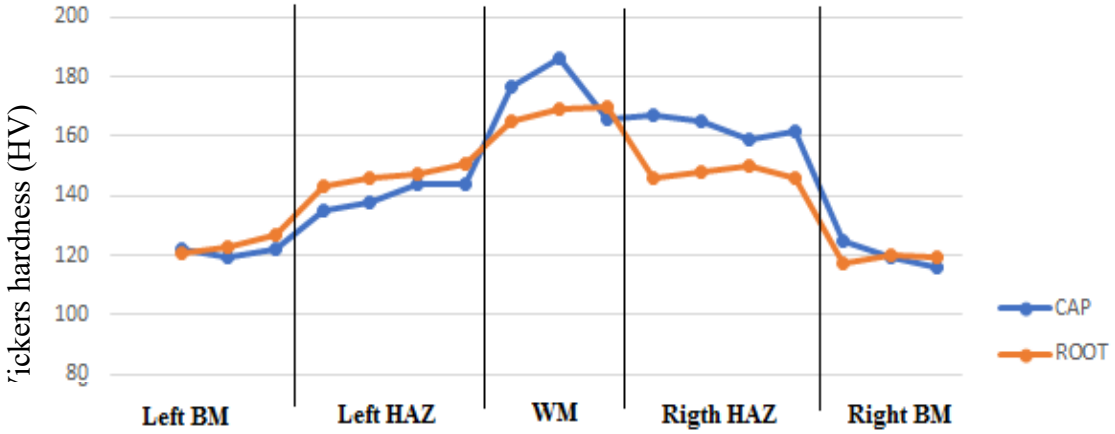

Fig. 2 - Hardness distribution curve in welded joint

Table 3 - Impact test result for test coupon

Test no.	Test temperature (°C)	Impact Energy (J)	Average impact energy (J)
1	-29	130	155
2		180	
3	-50	160	147
4		134	

4. Conclusion

In conclusion, the study has shown that SMAW process can produce a quality weld of low carbon steel ABS grade A marine plate with a heat input range of 0.15 kJ/mm to 1.71 kJ/mm. The welding parameters to achieve this heat input are welding voltage 23 V, welding current 70 A, and travel speed 88.24 mm/min to 666.67 mm/min. The weld quality is confirmed by the results of the visual inspection, radiographic test, microstructure examination, tensile test, side bend test, Charpy V-notch impact test, and microhardness test.

The metallurgical and mechanical behaviors of the weld were also studied. For the visual inspection test, the minor surface porosity is observed but it is still acceptable according to the AWS D1.1 standard. No visible defects were detected from the radiographic test. From microstructure examination, the grain size of weld metal is the finest as compared to the grain size of HAZ and the base metal. The ultimate tensile strength of the test specimen is higher than the minimum tensile strength of ABS Grade A steel plate, indicating a strong weldment has been achieved. The ultimate tensile strength of the test specimen is 522 MPa which is 6.3% higher than the minimum tensile strength of ABS Grade A steel plate of 491 MPa. For the side bend test, the test specimen shows a satisfactory result as the defect opening was 2.8 mm (max) which is still within the maximum acceptable defect range of 3.0 mm. For Charpy V-notch impact test, the test specimen achieves satisfactory results despite the unfavorable condition of -29 °C and -50 °C with an average impact energy of 155

J and 147 J respectively. For the microhardness test, the weld metal region has the highest hardness due to repeated heating and cooling during welding, while the base metal has the lowest hardness. The study provides valuable information for the welding industry, particularly for the fabrication of marine structures using low carbon steel ABS grade A marine plate.

References

[1] Phillips, D. Welding Engineering: An Introduction, John Wiley and Sons, Ltd., London, 2016.

[2] Baghel, P. K. (2022). Effect of SMAW process parameters on similar and dissimilar metal welds: An overview. *Heliyon*, e12161. Retrieved December 9, 2022 from https://doi.org/10.1016/j.heliyon.2022.e12161

[3] ISO. 9606-1:2012—Qualification Testing of Welders—Fusion Welding—Part 1: Steels; International Organization for Standardization: Geneva, Switzerland, 2012.

[4] Aalami-Aleagha, M. E. & Rashidi, A. M. (2012). Correlated macrostructural parameters of weld and weld current in the SMAW of small pipes, *J. Mech. Sci. Technol*., 26(1), pp. 181-185.

[5] Kumar, V., Albert, S. K., Chandrasekhar, N. & Jayapandian, J. (2018). Performance evaluation of arc welding process using weld data analysis, *T. Indian I. of Metals,* 71(12), pp. 3063-3075.

[6] de Sousa Lins, A., de Souza, L. F. G & M. C. Fonseca, M. C. (2018). Characterization of mechanical properties and residual stress in API 5L X80 steel welded joints, *J. Mater. Eng. Perform.*, 27(1), pp. 124-137.

[7] Boumerzoug, Z., Derfouf, C. & Baudin, T. (2010). Effect of welding on microstructure and mechanical properties of an industrial low carbon steel, *Engineering*, 2(7), pp. 502.

[8] Talabi, S., Owolabi, O., Adebisi, J. & Yahaya, T. (2014). Effect of welding variables on mechanical properties of low carbon steel welded joint, Adv. *Prod. Eng. Manage.,* 9(4), pp. 181-186.

[9] Asibeluo, S. & Emifoniye, E. (2015). Effect of arc welding current on the mechanical properties of A36 carbon steel weld joints, *Int. J. Mech. Eng. (SSRG-ISME)*, 2(9), pp. 32-40.

[10] Gharibshahiyan, E., Raouf, A. H., Parvin, N. & Rahimian, M. (2011). The effect of microstructure on hardness and toughness of low carbon welded steel using inert gas welding, *Mater. Des.*, 32(4), pp. 2042-2048.

[11] Kolhe, K. P. & Datta, C. K. (2008). Prediction of microstructure and mechanical properties of multipass SAW, *J. Mater. Process. Technol.*, 197(1-3), pp. 241-249.

[12] Muda, W. S. H. W., Nasir, N. S. M., Mamat, S. & Jamian, S. (2015). Effect of welding heat input on microstructure and mechanical properties at coarse grain heat affected zone of ABS grade A steel, *J. Eng. Appl. Sci.*, 10(20), pp. 9487-9495.

[13] Galvery, W. L. Welding essentials: questions & answers, Industrial Press Inc., New York, 2001.

[14] American Welding Society D1 Committee on Structural Welding, "Structural Welding Code-Steel," American National Standard AWS D1.1/D1.1M:2015, 23rd Ed., 2015

[15] Det Norske Veritas AS, "DNV Standard for Certification 2.7-1," Offshore Containers, 2013.

[16] "ASME Boiler and Pressure Vessel Code," The American Society of Mechanical Engineers, Section V, Nondestructive Examination, 2019.

[17] Standard Practice for Macroetching Metals and Alloys the American Society of Mechanical Engineers, ASTM E340, 2015.

[18] "Standard test methods and definitions for mechanical testing of steel products," Annual Book of ASTM Standards, A370, ASTM, West Conshohocken, PA, 2012.

[19] "Standard test method for guided bend test for ductility of welds," Annual Book of ASTM Standards, E190, ASTM, West Conshohocken, PA, 2008.

[20] "ASME Boiler and Pressure Vessel Code," The American Society of Mechanical Engineers, Section IX, Welding and Brazing Qualifications, 2007.

[21] "Standard Test Method for Notched Bar Impact Testing of Metallic Materials," Annual Book of ASTM Standards, E23-09, ASTM, West Conshohocken, PA, 2012.

[22] Leighly, H. P., Bramfitt, B. L. & Lawrence, S. J. (2001). RMS Titanic: A metallurgical problem, *Practical Failure Analysis,* 1(2)*,* pp. 10-13.

[23] "Standard Test Method for Microindentation Hardness of Materials," Annual Book of ASTM Standards, E384-16, ASTM, West Conshohocken, PA, 2016.

[24] Choubey, A. & Jatti, V. S. (2014). Influence of heat input on mechanical properties and microstructure of austenitic 202 grade stainless steel weldments, *WSEAS Transactions on Applied and Theoretical Mechanics,* 9, pp. 222-228.